Article
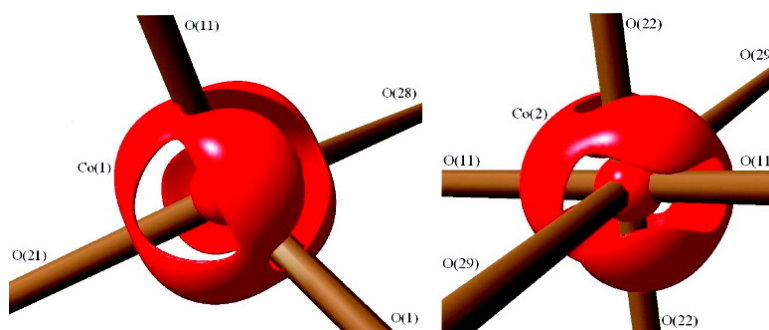
Synchrotron X-ray Charge Density Study of Coordination Polymer Co(CHO)(CHN)(CHNO) at 16 K

H. F. Clausen, J. Overgaard, Y. S. Chen, and B. B. Iversen

More About This Article

Additional resources and features associated with this article are available within the HTML version:

- Supporting Information
- Access to high resolution figures
- Links to articles and content related to this article
- Copyright permission to reproduce figures and/or text from this article

View the Full Text HTML

Synchrotron X-ray Charge Density Study of Coordination Polymer Co$_3$(C$_8$H$_4$O$_4$)$_4$(C$_4$H$_{12}$N)$_2$(C$_5$H$_{11}$NO)$_3$ at 16 K

H. F. Clausen,[†] J. Overgaard,[†] Y. S. Chen,[‡] and B. B. Iversen*,[†]

*Centre for Energy Materials, Department of Chemistry, and iNANO, University of Aarhus,
DK-8000 Aarhus C, Denmark, and ChemMatCARS, The University of Chicago, Advanced
Photon Source, Argonne, Illinois 60439*

Received January 29, 2008; E-mail: bo@chem.au.dk

Abstract: The charge density (CD) of coordination polymer Co$_3$(C$_8$H$_4$O$_4$)$_4$(C$_4$H$_{12}$N)$_2$(C$_5$H$_{11}$NO)$_3$ (**1**) has been determined from multipole modeling of structure factors obtained from single-crystal synchrotron X-ray diffraction measurements at 16 K. The crystal structure formally contains a negatively charged framework with cations and neutral molecules in the voids. However, the CD suggests that the framework is close to neutral, and therefore qualitative conclusions based on formal charge counting, e.g., about guest inclusion properties, will be incorrect. There are considerable differences in the charge distributions of the three unique benzenedicarboxylic acid linkers, which are widely used in coordination polymers. This suggests that the electrostatic properties of coordination polymer cavities, and thereby their inclusion properties, are highly tunable. The electron density topology shows that the tetrahedrally coordinated Co atom has an atomic volume which is 15% larger than that of the octahedrally coordinated Co atom. The crystal structure has both ferromagnetic and antiferromagnetic interactions, but no direct metal−metal bonding is evidenced in the CD. The magnetic ordering therefore takes place through superexchange in the oxygen bridges and the aromatic linkers. Bonding analysis of the experimental CD reveals that two oxygen atoms, O(1) and O(11), have significant covalent contributions to the metal−ligand bonding, whereas all other oxygen atoms have closed-shell interactions with the metals. This indicates that these two oxygen atoms are the key mediators of the magnetic ordering.

Introduction

During the past decade, numerous coordination polymers (CPs) have been synthesized with an amazing variety of structures.[1] The enormous interest is driven by the many attractive properties of these compounds. A primary feature of CPs compared with purely inorganic systems such as zeolites is that the fundamental building blocks (reactants) are preserved during self-assembly to form the CP product.[2] This offers a possibility for manipulating the structural configuration and thus the chemical and physical properties by changing the basic components, although explicit synthesis control can be difficult to obtain. Using solvothermal synthesis procedures, the specific product structures are often strongly dependent on synthesis parameters, such as pressure, time, concentration, and temperature.[3] Gas-storage applications have been a driving force in

many studies of CPs,[4] and nanoporous systems based on zinc coordinated by dicarboxylate or tricarboxylate linkers have shown promising results, with storage capabilities up to 7.5 wt % at 77 K.[5] This has naturally put emphasis of the guest inclusion properties of CPs and placed CPs as a fascinating class of host−guest systems. Effort is also currently being aimed at developing multifunctional CPs.[6] Our group has mainly focused on the magnetic properties of CPs.[7] The rational assembly of the basic building blocks may give novel systems for the fundamental study of the magnetic exchange mechanism, and by appropriate variation of the geometrical and electronic properties of the organic linker, it may be possible to fine-tune the magnetic interaction pathway. Studies of magnetic CPs are

[†] University of Aarhus.
[‡] The University of Chicago.

(1) (a) O'Keeffe, M.; Eddaoudi, M.; Li, H.; Reineke, T.; Yaghi, O. M. *J. Solid State Chem.* **2000**, *152*, 3–20. (b) Lu, J. Y. *Coord. Chem. Rev.* **2003**, *246*, 327–347. (c) Kitagawa, S.; Kitaura, R.; Noro, S. *Angew. Chem., Int. Ed.* **2004**, *43*, 2334–2375. (d) Ye, B.-H.; Tong, M.-L.; Chen, X.-M. *Coord. Chem. Rev.* **2005**, *249*, 545–565. (e) Bradshaw, D.; Claridge, J. B.; Cussen, E. J.; Prior, T. J.; Rosseinsky, M. J. *Acc. Chem. Res.* **2005**, *38*, 273–282. (f) Rosi, N. L.; Kim, J.; Eddaoudi, M.; Chen, B.; O'Keeffe, M.; Yaghi, O. M. *J. Am. Chem. Soc.* **2005**, *127*, 1504–1518.
(2) Yaghi, O. M.; O'Keeffe, M.; Ockwig, N. W.; Chae, H. K.; Eddaoudi, M.; Kim, J. *Nature* **2003**, *423*, 705–714.
(3) Clausen, H. F.; Poulsen, R. D.; Bond, A. D.; Chevallier, M.-A. S.; Iversen, B. B. *J. Solid State Chem.* **2005**, *178*, 3342–3351.

(4) (a) Chen, B.; Eddaoudi, M.; Hyde, S. T.; O'Keeffe, M.; Yaghi, O. M. *Science* **2001**, *291*, 1021–1023. (b) Eddaoudi, M.; Kim, J.; Rosi, N.; Vodak, D.; Wachter, J.; O'Keeffe, M.; Yaghi, O. M. *Science* **2002**, *295*, 469–472. (c) Kitaura, R.; Kitagawa, S.; Kubota, Y.; Kobayashi, T. C.; Kindo, K.; Mita, Y.; Matsuo, A.; Kobayashi, M.; Chang, H.-C.; Ozawa, T. C.; Suzuki, M.; Sakata, M.; Takata, M. *Science* **2002**, *298*, 2358–2361. (d) Dybtsev, D. N.; Chun, H.; Yoon, S. H.; Kim, D.; Kim, K. *J. Am. Chem. Soc.* **2004**, *126*, 523–527. (e) Zhao, X.; Xiao, B.; Fletcher, A. J.; Thomas, K. M.; Bradshaw, D.; Rosseinsky, M. J. *Science* **2004**, *306*, 1012–1015. (f) Lee, J. Y.; Li, J.; Jagiello, J. *J. Solid State Chem.* **2005**, *178*, 2527–2532. (g) Rowsell, J. L. C.; Spencer, E. C.; Eckert, J.; Howard, J. A. K.; Yaghi, O. M. *Science* **2005**, *309*, 1350–1354. (h) Dincă, M.; Dailly, A.; Liu, Y.; Brown, C. M.; Neumann, D. A.; Long, J. R. *J. Am. Chem. Soc.* **2006**, *128*, 16876–16883. (i) Panella, B.; Hirscher, M.; Pütter, H.; Müller, U. *Adv. Funct. Mater.* **2006**, *16*, 520–524.
(5) Wong-Foy, A. G.; Matzger, A. J.; Yaghi, O. M. *J. Am. Chem. Soc.* **2006**, *128*, 3494–3495.
(6) Kepert, C. J. *Chem. Commun.* **2006**, 695–700.

strengthened if nonmagnetic reference systems can be obtained,[8] but due to the different coordination properties of transition metals, this can be difficult to realize.[9]

Poulsen et al. reported the structure and physical properties of two completely isostructural nanoporous CPs, $M_3(C_8H_4O_4)_4(C_4H_{12}N)_2(C_5H_{11}NO)_3$ (M = Zn, Co), having complementary magnetic properties.[10] The structure of these compounds was described as three-atom metal chains interconnected by the deprotonated terephthalic acid units, resulting in a continuous three-dimensional framework. Two dimensions of the framework structure are more closely packed, which results in a layer-like structure with solvent-accessible voids between the layers. A formal charge count in the structure suggests a negatively charged framework, $M_3(C_8H_4O_4)_4^{2-}$, and cations ($C_4H_{12}N^+$, DEA) indeed occupy the voids. The diethylamine (DEA) ion is believed to form due to acid-catalyzed hydrolysis of the diethylformamide (DEF) molecule.[10] The voids also contain a DEF solvent molecule connected to the cationic DEA through hydrogen bonding. This removes disorder in one of the ethyl branches, resulting in partial ordering of the DEF molecule. A second DEF molecule is situated in the void, but this molecule has no strong bonding interaction to the neighboring solvent molecules nor to the framework structure. It is important to note that the Zn and Co compounds also are completely isostructural with regard to the guest molecules in the nanopores. The Co—O bond lengths were found to be slightly longer than the corresponding Zn—O bonds, with the exception of Co(2)—O(11), in which the opposite was observed.[10] Based on multi-temperature single-crystal X-ray diffraction data, it was proposed that a further shortening of this bond would be seen below 100 K.[10]

Poulsen et al. also reported magnetic susceptibility and heat capacity data measured between 2 and 350 K, and a clear phase transition was observed at temperatures below 10 K. Furthermore, an anomaly of unknown origin was observed at 50 K. A fit to the Curie—Weiss law for the data above 60 K gave a Weiss temperature of 23 K and an effective moment of 4.2 μ_B. Measurement of the magnetization in different fields suggested that the low-temperature phase transition is a ferromagnetic ordering of the Co^{2+} moments.

In the present study, we attempt to combine information about the microscopic electronic structure obtained from multipole modeling of single-crystal synchrotron X-ray diffraction data with the macroscopic physical property data stemming from the study by Poulsen et al.[10] The present study is a strong example of the immense advances in experimental charge density (CD) analysis provided by intense third-generation synchrotrons. Due to severe crystal twinning, it has been challenging to find a single crystal suitable even just for structure determination of **1**, and the structure reported by Poulsen et al. was also based on synchrotron measurements.[10] Charge density analysis requires

measurement of Bragg intensities to much higher order than structure determination, and such intensities are simply not observable using conventional X-ray sources with the available crystals. It is the use of a very powerful insertion device at a third-generation synchrotron source that provided the key to a successful measurement of a CD quality data set. So far, it has not been possible to obtain crystals suitable for X-ray CD analysis of the nonmagnetic reference Zn compound.

Experimental Section

Synthesis. The synthesis of the compound $[Co_3(C_8H_4O_4)_4]^{2-}[C_4H_{12}N]^+_2 \cdot 3C_5H_{11}NO$ (**1**) is a one-pot solvothermal reaction. A mixture of $CoCl_2 \cdot 6H_2O$ (0.294 g, 1 mmol) and DEF (2 mL) was added to a mixture of 1,4-benzenedicarboxylic acid (H_2BDC, 0.166 g, 1 mmol) and DEF (8 mL). This mixture was sealed in a 12 mL Teflon autoclave at 375 K for 72 h, which resulted in small, rhombic-shaped purple crystals.

Synchrotron X-ray Data Collection. The crystals of **1** show a tendency for twinning due to the layering of thin plates; therefore, a number of crystals had to be tested before a suitable specimen was found. The selected purple crystal (0.020 × 0.020 × 0.050 mm³) was mounted in epoxy glue on the tip of a glass fiber rod glued to a small cobber wire. Using a brass pin and a goniometer head, this was mounted on a HUBER four-circle diffractometer at the ChemMatCARS beamline (ID-15) at the Advanced Photon Source, Argonne National Laboratory (Argonne, IL). The data collection was carried out using a wavelength of 0.413 Å obtained from a diamond (111) monochromator. The crystal was cooled to 16(2) K using a Pinkerton-type helium cooling device.[11] The data collection was performed in φ-scan mode using steps of 0.3° and with fixed ω- and χ-angles. An exposure time of 1 s was sufficient to obtain significant intensity in the high-order data without saturating the Bruker 6000 CCD-based detector with the intense low-order data. The detector was placed 7.36 cm from the crystal, and the measurements were performed at two different 2θ settings (20° and 33°), yielding a maximum resolution of 1.26 Å⁻¹. A total of 167 899 reflections were collected and integrated with SAINT+.[12] These integrated intensities were corrected for the imperfect detection of the CCD phosphor (oblique incidence correction),[13] and SADABS[12] was used to correct for slight misalignment of the crystal with the φ-axis, as well as other effects. An empirical absorption correction and data averaging was done using SORTAV,[14] yielding a total of 37 951 unique reflections with R_{int} = 5.6%. The combined use of high energy X-rays (30 keV) and a small crystal provides a data set in which systematic errors such as absorption and extinction are strongly reduced. Furthermore, in an attempt to avoid the influence of multiple scattering effects and spurious single-measurement outliers, only reflections measured three times or more are used in the least-squares refinements. More experimental details can be found in Table 1 and the Supporting Information.

Multipole Refinement. The direct methods program SHELXS was used to solve the structure from the diffraction data.[12] As recently reported, the isostructural Zn compound exhibits solvent molecule disorder at 30 K,[10] and this is also observed for **1** at 16(2) K. The occupancy of the disordered groups in the solvent molecules was fixed at values obtained from the independent atom model (IAM) refinement in SHELXL, in which the occupancies of different configurations of the molecules are refinable parameters.

(7) (a) Poulsen, R. D.; Bentien, A.; Graber, T.; Iversen, B. B. *Acta Crystallogr., Sect. A* **2004**, *60*, 382–389. (b) Poulsen, R. D.; Bentien, A.; Chevallier, M.; Iversen, B. B. *J. Am. Chem. Soc.* **2005**, *127*, 9156–9166. (c) Poulsen, R. D.; Jørgensen, M. R. V.; Overgaard, J.; Larsen, F. K.; Morgenroth, W.; Graber, T.; Chen, Y.; Iversen, B. B. *Chem. Eur. J.* **2007**, *13*, 9775–9790.
(8) Tynan, E.; Jensen, P.; Kelly, N. R.; Kruger, P. E.; Lees, A. C.; Moubaraki, B.; Murray, K. S. *Dalton Trans.* **2004**, 3440–3447.
(9) Clausen, H. F.; Overgaard, J.; Poulsen, R. D.; Morgenroth, W.; Iversen, B. B. *Acta Crystallogr., Sect. E* **2006**, *62*, 3333–3335. Poulsen, R. D.; Overgaard, J.; Chevallier, M.-A.; Clausen, H. F.; Iversen, B. B. *Acta Crystallogr., Sect. E* **2005**, *61*, 1337–1339.
(10) Poulsen, R. D.; Bentien, A.; Christensen, M.; Iversen, B. B. *Acta Crystallogr., Sect. B* **2006**, *62*, 245–254.

(11) Hardie, M. J.; Kirschbaum, K.; Martin, A.; Pinkerton, A. A. *J. Appl. Crystallogr.* **1998**, *31*, 815–817.
(12) Sheldrick, G. M. SAINT+, SADABS, XPREP and SHELXTL programmes included in the *Bruker SMART CCD* software, 2003.
(13) (a) Iversen, B. B.; Larsen, F. K.; Pinkerton, A. A.; Martin, A.; Darovsky, A.; Reynolds, P. A. *Acta Crystallogr., Sect. B* **1999**, *55*, 363–374. (b) Wu, G.; Rodrigues, B. L.; Coppens, P. *J. Appl. Crystallogr.* **2002**, *35*, 356–359.
(14) Blessing, R. H. *J. Appl. Crystallogr.* **1997**, *30*, 421–426.

Table 1. Crystallographic Details

	1
empirical formula	$Co_3O_{19}N_5C_{55}H_{73}$
formula weight (g/mol)	1284.98
space group	*C2/c*
T (K)	16(2)
a (Å)	33.1947(16)
b (Å)	9.7794(4)
c (Å)	18.2274(7)
β (°)	92.520(1)
V (Å^3)	5911.3(4)
μ (mm^{-1})	0.179
T_{min}/T_{max}	0.988, 1.000
N_{meas}	167899
R_{int} ($S < 0.8$ Å^{-1}, all data)	0.0431, 0.0562
$R(\sigma)$	0.081
$\sin(\theta_{max})/\lambda$ (Å^{-1})	1.264
$N_{obs}(2\sigma)$	18635
N_{par}	1005
$R_{all}(F)$, $R_{all}(F^2)$	0.038, 0.038
GoF	0.63

The initial structural model obtained from SHELXL (atomic positions and displacement parameters) was refined against those high-order data having values of $\sin(\theta)/\lambda > 0.8$ Å^{-1}. Subsequently, the electron density was refined with a multipole model using the program XD.[15] The structural parameters obtained in the high-order refinement were fixed during the initial refinement of the multipole parameters. However, the final model included a simultaneous refinement of all structural and electronic parameters of the ordered atoms. The maximum correlation parameter in the refinement was between displacement parameters of the disordered DEF molecules, and these parameters were varied in separate cycles. The non-spherical electron density model included all atoms of the framework, the ordered DEA molecule, and one of the two disordered unique DEF molecules. The multipole-modeled disordered DEF molecule is hydrogen-bonded to the cationic DEA, and it cannot be excluded from the model due to possible charge transfer. The parameters of the disordered ethyl group of this DEF molecule were constrained to the values of the ordered ethyl group within the same solvent molecule. The other DEF solvent molecule is disordered into four positions, and it was kept with spherical atoms. Since all interatomic distances to this strongly disordered DEF molecule are long (the shortest distance is 2.2 Å between O(71A) and H(33a) or 1.57 Å between H(71a) and H(33c)), it appears to have very weak intermolecular bonding, and thus it is reasonable to assume that this molecule is neutral and has zero charge transfer to the surrounding moieties. The final model of the refined atoms included hexadecapoles on cobalt and octupoles on all other non-hydrogen atoms, as well as a monopole and a bond-directed dipole on all H-atoms. The radial function of a Co^{2+} ion (d^7) taken from the SCM scattering bank in XD was employed for the transition metal sites.[16] The positions of the hydrogen atoms were reset after each refinement cycle to equal standard average neutron diffraction results.[17] Two radial expansion/contraction parameters (κ' and κ'') were introduced for each chemically unique type of atom, giving the following final values: $\kappa'(Co(1)) = 0.994(4)$, $\kappa''(Co(1)) = 0.715(13)$, $\kappa'(Co(2)) = 0.993(5)$, $\kappa''(Co(2)) = 0.702(18)$, $\kappa'(N) = 0.997(4)$, $\kappa''(N) = 0.82(3)$, $\kappa'(O) = 0.983(2)$, $\kappa''(O) = 0.695(18)$, $\kappa'(C(sp^2)) = 0.978(3)$, $\kappa''(C(sp^2) = 0.928(10)$, $\kappa'(C(sp^3)) = 0.937(4)$,

and $\kappa''(C(sp^3)) = 0.887(15)$. Expansions of the model were tested, including anharmonic displacement tensors and additional κ parameters. However, the residual density maps did not improve, and the extra parameters were discarded. Similarly, extinction was found to be insignificant, and the final model included 1005 parameters refined against 18 635 observations ($I > 2\sigma(I)$). The Hirshfeld rigid bond test was satisfactorily fulfilled for all parts of the ordered structure, with the mean value of the difference of mean-square displacement amplitudes (DMSDA) being $\Delta_{A-B} = 3.1$ pm^2 (the maximum value was 12 pm^2).[18] A full list of DMSDA values is deposited in the Supporting Information. The residual density plots exhibit extremes near the two cobalt atoms ($\sim$0.4 e Å^{-3} when using all data). Recently, we studied in detail the effects on refinement residuals of removing outlier reflections based on their deviations from values calculated from a multipole model.[19] It was found that such approaches easily decrease the residuals by a factor of 2, without affecting the refined multipole model. Furthermore, it was established that only very weak, primarily high-angle reflections were discarded by this procedure; hence, a similar effect is obtained by truncating the calculation of difference Fourier maps at some chosen resolution, thereby actually creating a more reliable view of the errors in the experiment and an increased ability to identify model flaws. Accordingly, Figure 1 shows the residual density maps using only data below a resolution of 0.8 Å^{-1}, while maps calculated from all reflections are given in the Supporting Information.

Results and Discussion

Structure of 1. The structure of the coordination polymer consists of three-atom chains of carboxylate-bridged cobalt atoms bridged by three unique benzenedicarboxylic acid linkers, denoted BDCI, BDCII, and BDCIII. The discrete Co chain consists of a tetragonally distorted, octahedrally coordinated Co atom (Co(2)) situated at an inversion center in the space group and a distorted, tetrahedrally coordinated cobalt, Co(1), at each end of the chain (see Figure 2). Selected bond distances are listed in Table 2. The framework is more densely packed in two dimensions due to the cross-linking of the discrete metal chains by the BDCI and BDCII linkers, thus resulting in a layer-like structure (see Figure 2C). These layers are connected by the BDCIII linker, resulting in a 3D framework.

The BDCI linker contains two almost completely delocalized carboxylate groups bridging two neighboring cobalt atoms (O(21), O(22), O(28), and O(29) in Table 2). The carboxylate groups of BDCII and BDCIII are partly localized, and these groups bond to the metal centers with only one oxygen atom each. The carboxylate group of BDCII connects the two unique Co atoms via a direct oxygen bridge (O(11)), while the carboxylate group of BDCIII is bonded only to Co(1) through O(1). As mentioned above, a formal charge count yields a negatively charged framework, and hence the solvent molecules formally are cationic. However, the analysis of the CD will show if there is charge transfer between the host framework and the guest molecules. The coordination of Co(1) is distorted tetrahedral, with a formal charge of +1.75, and the coordination of Co(2) is tetragonally distorted octahedral, with a formal charge of +2.50, if all oxygen atoms in the carboxylate groups share the negative charges.[10] On the basis of the synthesis conditions, we expect cobalt to be in the +2 valence state as the starting material was $CoCl_2 \cdot 6H_2O$, but the atomic charges derived from the CD can be used to verify this.

(15) Koritsanszky, T.; Howard, S. T.; Richter, T.; Macchi, P.; Volkov, A.; Gatti, C.; Mallinson, P.; Farrugia, L. J.; Su, Z.; Hansen N. K. *XD.—A Computer Program Package for Multipole Refinement, Topological Analysis of Charge Densities from Diffraction Data,* 2003.

(16) (a) Su, Z.; Coppens, P. *Acta Crystallogr., Sect. A* **1998**, *54*, 646–652. (b) Macchi, P.; Coppens, P. *Acta Crystallogr., Sect. A* **2001**, *57*, 656–662.

(17) Allen, F. H.; Kennard, O.; Watson, D. G.; Brammer, L.; Orpen, A. G.; Taylor, R. *J. Chem. Soc., Perkin Trans. 2* **1987**, 1–19.

(18) (a) Harel, M.; Hirshfeld, F. L. *Acta Crystallogr., Sect. B* **1975**, *31*, 162–172. (b) Hirshfeld, F. L. *Acta Crystallogr., Sect. A* **1976**, *32*, 239–244.

(19) Overgaard, J.; Clausen, H. F.; Platts, J. A.; Iversen, B. B. *J. Am. Chem. Soc.* **2008**,
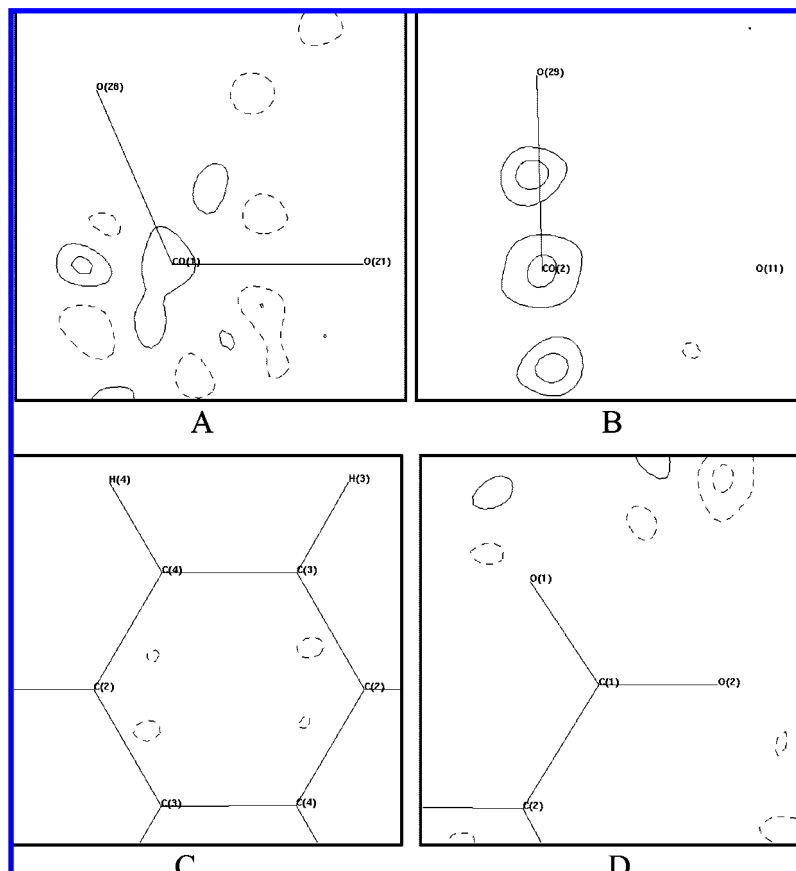
Figure 1. Residual maps obtained with a cutoff value of 0.8 Å^{-1}. The maps include (A) the Co(1)−O(28)−O(21) plane, (B) the Co(2)−O(29)−O(11) plane, (C) the BDCIII linker, and (D) a carboxylate group of BDCIII. The contour intervals are 0.1 e Å^{-3}, and solid contours are positive.
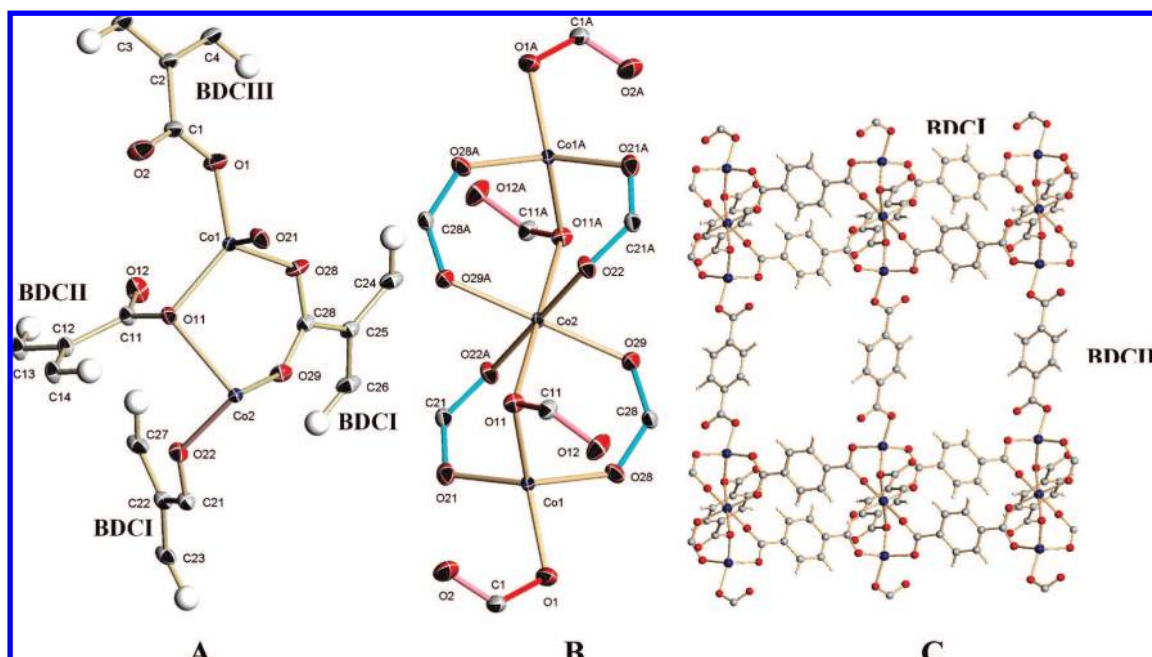

Figure 2. (A) Asymmetric unit of the framework of **1**. (B) Coordination of the three metal atoms in the chain. The turquoise bonds are fully delocalized, while the red bonds are longer in the partially localized carboxylate groups. (C) Framework channels of the layered structure viewed along the *b*-axis of the unit cell, where the solvent molecules have been omitted for clarity. The thermal ellipsoids are drawn at a 90% level.

On the basis of the behavior of the isostructural Zn analogue to **1**, Poulsen et al. suggested that the carboxylate twist (defined by the torsion angle O(11)−C(11)−C(12)−C(13)) in the BDCII linker as well as the bond length of Co(2)−O(11) will decrease at lower temperature (Table 2). This is indeed found to be the case, with Co(2)−O(11) decreasing from 2.217(2) to 2.2071(4) Å, whereas the twist angle changes from 0.5(3)° to 0.12(8)°. The bond length and twist of Co(2)−O(11) presumably correlate

Table 2. Selected Bond Distances (Å) for **1**

	16 K	120 K[a]
Co(1)−Co(2)	3.22685(7)	3.239(3)
Co(1)−O(1)	1.9392(4)	1.940(3)
Co(1)−O(11)	1.9913(4)	1.998(2)
Co(1)−O(21)	1.9801(6)	1.982(2)
Co(1)−O(28)	1.9723(5)	1.979(2)
Co(2)−O(11)	2.2071(4)	2.217(2)
Co(2)−O(22)	2.0489(5)	2.053(2)
Co(2)−O(29)	2.0301(5)	2.040(2)
O(21)−C(21)	1.2678(6)	1.277(4)
O(22)−C(21)	1.2572(7)	1.259(4)
O(28)−C(28)	1.2668(6)	1.270(4)
O(29)−C(28)	1.2551(6)	1.260(4)
O(1)−C(1)	1.2907(7)	1.295(4)
O(2)−C(1)	1.2381(8)	1.236(4)
O(11)−C(11)	1.2986(7)	1.307(4)
O(12)−C(11)	1.2379(8)	1.243(4)

[a] Data from ref 10.
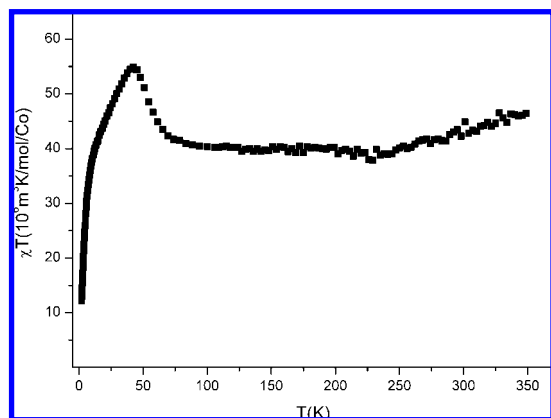
Figure 3. Temperature dependence of χT from 2 to 300 K.

with the magnetic interaction, which may originate from the π-orbital of the carboxylate linkers being oriented toward the d-orbitals of the cobalt atoms to interact in a superexchange mechanism.

Physical Properties. Poulsen et al. noted an anomaly in the magnetic susceptibility measurements of **1** at 50 K, which was proposed to be an onset of magnetic ordering.[10] Therefore, only data above 60 K were fitted to a Curie−Weiss expression, giving a Weiss temperature, Θ, of 23 K and an effective moment of 4.2 μ_B. Measurements of the magnetization as a function of field at different temperatures suggested a ferromagnetic ordering of Co^{2+} ions ($\mu_{sat} \approx 3 \mu_B$), and a sharp rise in magnetization with increasing field is observed below 10 K.[10] The heat capacity reveals a phase transition at 6 K, which is in good agreement with the magnetic ordering. A new plot of the magnetic susceptibility data is shown in Figure 3.

The χT plot reveals different types of interactions, as ferromagnetic, antiferromagnetic, and paramagnetic interactions are accompanied by an increase, decrease, and constant value in χT, respectively.[20] A ferromagnetic region is seen for temperatures between ∼85 and ∼42 K. Prior to the ferromagnetic ordering, a flat plateau is found, which corresponds to the paramagnetic state. Fitting of data points above 100 K gives a Weiss temperature of 5.6 K and an effective moment of 4.9 μ_B, in agreement with the heat capacity data. Below ∼42 K,

the value of χT decreases in two steps, with the second step being at ∼10 K. The drop in χT for $T < 42$ K presumably is due to antiferromagnetic ordering of **1**. From the different magnetic interactions, it appears that the Co ions have several interaction pathways available in the complex crystal structure.
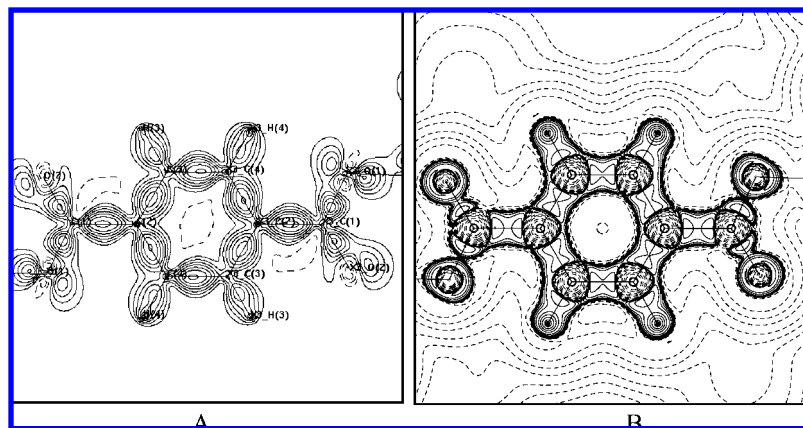
Charge Density. The static deformation density and Laplacian distribution of one of the BDC linkers is shown in Figure 4, while static deformation densities of metal−ligand planes are shown in Figure 5. Additional plots are deposited in the Supporting Information.

The static deformation map in Figure 4 shows single peak maxima in aromatic bonds and overall demonstrates that the present model density is of high quality. The metal−ligand planes in Figure 5 reveal that the Co atoms have clear deviations from the spherical distribution of the independent atom model. All metal−ligand interactions, except the Co(1)−O(1) and Co(1)−O(11) bonds, are characterized by a negative metal region pointing toward a positive ligand region. The Co(1)−O(1) and Co(1)−O(11) interactions, on the other hand, seem to have some covalent contributions to the bonding, with charge accumulation in the bond.

Bonded atoms are connected through a line of maximum electron density, and a bond critical point (bcp) appears at the local minimum of ρ along this line. A complete list of bcps is deposited in the Supporting Information, while Table 3 gives the topological properties in the Co ligand bonds only. No bond path can be found between Co(1) and Co(2), but a ring critical point is located in this region. Thus, there is no direct bonding interaction between the cobalt atoms which can mediate magnetic ordering, and this must therefore occur through the linking organic molecules.

The ρ_c values in the Co−O bonds range from 0.25 to 0.67 e Å^{-3}, and the Laplacian is always positive. It is noteworthy that the Co(1)−O(1) and Co(1)−O(11) bonds exhibit negative H values. This indicates that these bonds possess a larger degree of covalency than the remaining Co−O bonds, which all show positive values of H.[22] A plot of $\nabla^2\rho_c$ versus M−O distance for various transition metal bonds (Fe−O, Mn−O, Co−O, Figure 6A) follows a clear exponential decrease, as is also observed in closed-shell hydrogen bonds.[23] In the early literature on topological analysis of chemical bonding, it was argued that a $(G/\rho)_c$ value above unity is a signature of closed-shell bonding.[24] This is observed for all the Co−O bonds in **1**. However, Gibbs and co-workers recently examined a range of commonly used measures for characterizing chemical bonding.[25] It was shown that for M−O bonds, where M is a non-transition metal, the $(G/\rho)_c$ value is above unity and actually increases with decreasing bond length. Furthermore, the increase in $(G/\rho)_c$ is clearly accompanied by an increasing covalent character of the bonding. In Figure 6B, $(G/\rho)_c$ is plotted for a range of transition metal−oxygen bonds on the basis of experimental CD studies from our group.[26] The trend is clear that also for transition metal−oxygen bonds, $(G/\rho)_c$ increases with decreasing bond length. It is of interest to probe in detail whether the increase in $(G/\rho)_c$ for transition metal−oxygen bonds is also accompanied by an increasing

(20) Konar, S.; Mukherjee, P. S.; Drew, M. G. B.; Ribas, J.; Chaudhuri, N. R. *Inorg. Chem.* **2003**, *42*, 2545–2552.

(21) Abramov, Y. *Acta Crystallogr., Sect. A* **1997**, *53*, 264–272.
(22) Macchi, P.; Sironi, A. *Coord. Chem. Rev.* **2003**, *238−239*, 383–412.
(23) Espinosa, E.; Alkorta, I.; Elguero, J.; Molins, E. *J. Chem. Phys.* **2002**, *117*, 5529.
(24) Bader, R. F. W.; Essen, H. *J. Chem. Phys.* **1984**, *80*, 1943.
(25) Gibbs, G. V.; Spackman, M. A.; Jayatilaka, D.; Rosso, K. M.; Cox, D. F. *J. Phys. Chem. A* **2006**, *110*, 12259–12266.

Figure 4. Static deformation density (A) and Laplacian distribution (B) of the BDCIII linker. For the deformation density, the contour interval is 0.1 e Å^{-3}, with solid contours being positive and dashed contours negative. For the Laplacian map, the contour level is $2^x \times 10^y$ ($x = 0, 1, 2, 3$ and $y = -2, -1, 0, 1, 2, 3$), with dashed lines being positive values and solid lines negative.
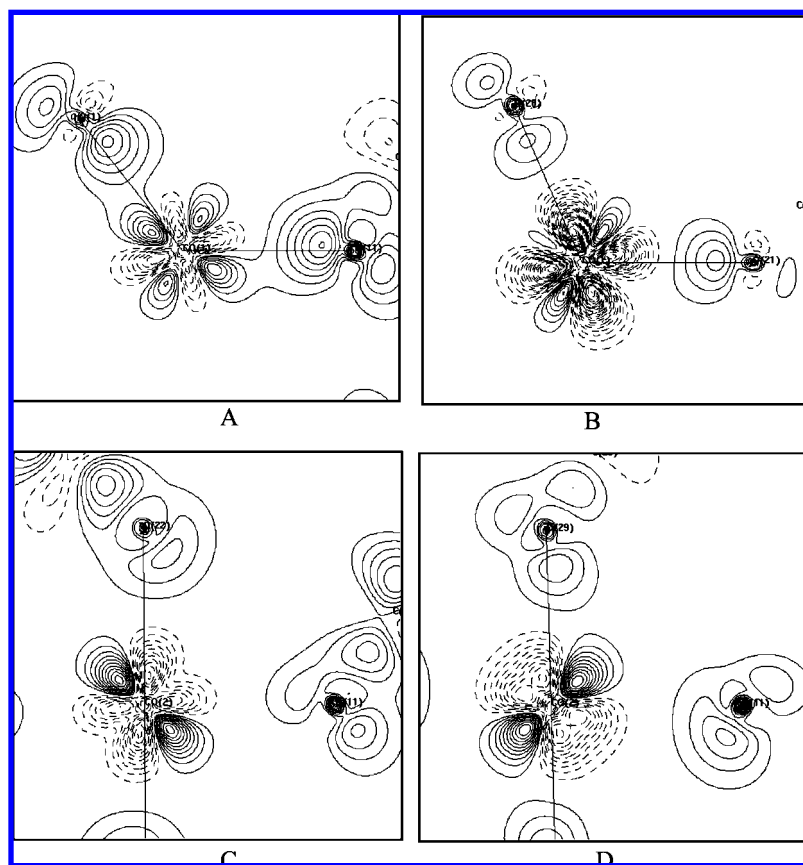
Figure 5. Static deformation density maps of (A) the Co(1)−O(1)−O(11) plane, (B) the Co(1)−O(21)−O(28) plane, (C) the Co(2)−O(11)−O(22) plane, and (D) the Co(2)−O(11)−O(29) plane. The contour interval is 0.1 e Å^{-3}, with solid contours being positive and dashed contours negative.

covalent character of the bonding. The Co−O(1) and Co−O(11) bonds do not stick out as having particularly high $(G/\rho)_c$ values, but the analysis by Gibbs et al. suggests that the high $(G/\rho)_c$ values are compatible with significant covalency in the bonding.

According to the zero flux condition, atoms can be separated into discrete, non-overlapping atomic basins from which atomic properties can be derived. One particularly appealing feature of this partitioning is that atomic properties such as energy, volume, and charge are additive.[27] The properties of selected atoms in **1** are shown in Table 4, and a complete list is given in the Supporting Information.

Summation of the topological charges in the framework results in an overall almost neutral network with a charge of +0.07, suggesting that significant charge transfer has occurred from the formally negative framework structure to the cationic solvent molecules. Due to the disorder of the solvent molecules, it is difficult to locate the atomic surfaces in the cavities, and the solvent molecule charges are poorly defined. The charge neutrality of the framework is an important observation, since studies of coordination polymers often touch on the formal charge state of a given framework. This is to a large part due to the expectation that the inclusion properties of a given framework will depend strongly on the charge distribution and

Table 3. Topological Measures at the Bond Critical Points[a]

bond	R	R_{12}	$d_{1\text{-bcp}}$	ρ_c	$\nabla^2\rho_c$	G/ρ	H/ρ	$|V|/G$
Co(1)−O(1)	1.9392(4)	1.940	0.965	0.67	13.3	1.54	−0.15	1.10
Co(1)−O(11)	1.9913(4)	1.993	0.975	0.56	11.6	1.51	−0.07	1.05
Co(1)−O(21)	1.9801(6)	1.989	0.955	0.46	11.6	1.64	0.11	0.95
Co(1)−O(28)	1.9723(5)	2.014	0.967	0.39	10.6	1.69	0.20	0.89
Co(2)−O(11)	2.2071(4)	2.215	1.082	0.25	5.6	1.38	0.20	0.85
Co(2)−O(22)	2.0489(5)	2.056	0.997	0.35	9.4	1.65	0.23	0.86
Co(2)−O(29)	2.0301(5)	2.039	0.987	0.41	9.6	1.53	0.10	0.94

[a] R is the bond distance between the two atoms, and R_{ij} is the sum of the distance from first atom through the bcp to the other atom (Å). $d_{1\text{-bcp}}$ (Å) is the distance from the bcp to the atom. ρ_c (e/Å^3) is the electron density, and $\nabla^2\rho_c$ (e/Å^5) is the Laplacian at the bcp. G, H, and V are the local kinetic, the local potential, and the total energy density (Hartree Å^{-3}) derived using the Abramov approximation.[21] The random errors of ρ_c and $\nabla^2\rho_c$ estimated from the least-squares refinement are significant underestimates of the real error, and they are therefore not listed. Instead, values of ρ_c are presented with two decimals, while the Laplacian values are truncated after the first decimal.

the corresponding electrostatic properties. In other words, the electrostatic potential in the cavities will be highly dependent on the charge state of the framework. Recently, theoretical calculations have started addressing the mechanism of gas storage in CPs based on electrostatic interactions,[28] and it would be of considerable interest to compare the experimental CD of **1** with results from theory, but ab initio theoretical calculations on **1** are highly challenging. In the present case, formal charge counting is inaccurate, and potential conclusions based on the framework being negative therefore would be in error. The significant charge reorganization between the framework and the guest atoms probably can explain why there are significant differences in the thermal decomposition patterns between the isostructural Zn and Co analogues.[10] The release of the solvent molecules in the cavities occurs both at different temperatures in the two compounds and with different enthalpies. In both compounds, a stable plateau in the TGA/DSC is reached at ∼600 K, which presumably corresponds to the naked framework.[10] It may be the neutrality of the framework that makes it possible to obtain a stable naked configuration, since a solid cannot have an overall negative charge. Summation of the topological charges for the different BDC linkers reveals substantial differences. The intralayer linkers BDCI and BDCII are considerably more negatively charged than the interlayer linker BDCIII. This is due to the carboxylate group of BDCIII being less negatively charged, while the benzene ring of the BDCIII linker is positively charged. The intralayer linkers all have negatively charged benzene rings. The considerable differences in the BDC charge distributions is a strong indication that the electrostatic properties, and thereby the guest inclusion properties, are tunable.

The atomic charges of Co(1) and Co(2) are quite similar, with values of +1.88 and +1.91, which agrees well with the expected charge of +2. On the other hand, the mixed valence

(26) (a) Overgaard, J.; Hibbs, D. E.; Rentschler, E.; Timco, G. A.; Larsen, F. K. *Inorg. Chem.* **2003**, *42*, 7593–7601. (b) Overgaard, J.; Larsen, F. K.; Schiøtt, B.; Iversen, B. B. *J. Am. Chem. Soc.* **2003**, *125*, 11088–11099. (c) Poulsen, R. D.; Bentien, A.; Graber, T.; Iversen, B. B. *Acta Crystallogr., Sect. A* **2004**, *60*, 382–389. (d) Poulsen, R. D.; Bentien, A.; Chevallier, M.; Iversen, B. B. *J. Am. Chem. Soc.* **2005**, *127*, 9156–9166.
(27) Bader, R. F. W. *Atoms in molecules. A quantum theory*; Clarendon Press: Oxford, 1990.
(28) Belof, J. L.; Stern, A. C.; Eddaoudi, M.; Space, B. *J. Am. Chem. Soc.* **2007**, *129*, 15202–15210.
(29) Hübschle, C. B.; Luger, P. *J. Appl. Crystallogr.* **2006**, *39*, 901–904.

Table 4. Integrated Atomic Properties[a]

	monopole charge	Bader charge	TBV	ΔTBV	dipole moment
Co(1)	2.07	1.88	66.6	0.7	0.03
Co(2)	2.05	1.91	58.1	0.0	0.00
sum	3.095	2.835			
BDCI					
O(21)	−0.23	−1.06	106.4	5.5	0.23
O(22)	−0.18	−1.07	102.6	6.9	0.31
C(21)	−0.29	1.49	39.3	3.4	0.75
C(22)	−0.12	−0.15	80.6	13.6	0.11
C(23)	−0.32	−0.23	89.5	10.0	0.39
C(24)	−0.28	−0.19	92.4	13.7	0.39
C(25)	−0.17	−0.22	76.6	6.7	0.04
C(26)	−0.21	−0.14	92.4	15.1	0.39
C(27)	−0.26	−0.21	99.1	21.6	0.34
C(28)	−0.26	1.58	39.9	5.3	0.72
O(28)	−0.27	−1.12	105.9	5.6	0.48
O(29)	−0.25	−1.17	105.7	11.2	0.38
H(23)	0.26	0.25	33.8	2.6	0.14
H(24)	0.3	0.25	35.9	1.9	0.18
H(26)	0.25	0.20	50.6	18.6	0.17
H(27)	0.28	0.23	36.7	5.0	0.17
sum	−1.75	−1.56			
BDCII					
O(11)	−0.33	−1.0	89.5	4.5	0.26
O(12)	−0.18	−1.14	116.1	11.0	0.37
C(11)	−0.24	1.47	38.1	3.2	0.73
C(12)	−0.16	−0.17	77.8	10.5	0.06
C(13)	−0.26	−0.2	92.8	14.4	0.35
C(14)	−0.38	−0.31	94.1	14.9	0.34
H(13)	0.26	0.22	51.2	19.8	0.15
H(14)	0.3	0.22	34.2	1.5	0.20
sum	−0.99	−0.91			
BDCIII					
O(1)	−0.17	−0.86	94.2	1.4	0.22
O(2)	−0.12	−1.08	118.2	7.6	0.55
C(1)	−0.26	1.44	34.5	0.0	0.64
C(2)	−0.15	−0.19	67.2	0.8	0.07
C(3)	−0.25	−0.05	74.9	3.0	0.54
C(4)	−0.26	0.02	75.4	4.8	0.54
H(3)	0.29	0.24	37.8	3.8	0.19
H(4)	0.24	0.18	34.1	1.5	0.15
sum	−0.68	−0.3			
total	−0.32	0.07			

[a] For comparison, atomic charges estimated from refined monopole populations are also listed. TBV is the total basin volume (Å^3), whereas ΔTBV is the difference between the total basin volume and the volume of the basin having an electron density above 0.002 au. The sum of the separate units is found by adding the atomic contributions, and the total sum of the framework of **1** is given as obtained by by adding the separate units.

charges of +2.50 and +1.75 obtained from a formal charge count assuming delocalized carboxylate groups are clearly incorrect. As expected for the highly symmetric Co(2) atom, the atomic dipole moment is close to zero, whereas for the tetrahedrally distorted Co(1), a larger first moment is found, in correspondence with the more asymmetric coordination. Even though the expansion/contraction parameters and the atomic charges of the two cobalt atoms are similar, there is a substantial difference in their respective atomic volumes, with the tetrahedral Co atom being about 15% larger than the octahedral Co atom. The average electron density consequently is smaller in the Co(1) basin. For close-packed structures, it is often argued that larger cations will be located in octahedral holes, since these are larger than their tetrahedral counterparts. In the present CP, the tetrahedrally coordinated atoms are nevertheless largest. The different shapes of the two cobalt atom charge distributions are

Figure 6. (A, left) Experimental values of $\nabla^2\rho_c$ as a function of metal−oxygen bond length based on the present study as well as literature values.[26] The blue triangles are from three carboxylate bridged trinuclear iron complexes, black squares from an iron containing butterfly like complexes, red dots from two manganese metal organic frameworks and green triangles are from **1** with Co−O bonds. (B, right) $(G/\rho)_c$ versus bond length for the same bonds as in (A).
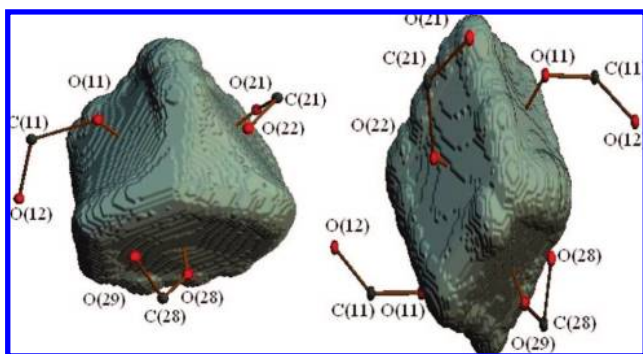
Figure 7. Atomic surfaces of the two cobalt atoms determined from the experimental charge density distribution: left, Co(1); right, Co(2).

visualized in Figure 7, which shows the zero flux surfaces of the two atoms.

The oxygen atoms of **1** can be divided into several different types on the basis of their bonding to the cobalt atoms. Bridging of delocalized carboxylate groups is exclusively observed in the BDCI linker (O(21), O(22), O(28), and O(29)). In BDCII and BDCIII, there are four different types of oxygen atoms: one hydrogen-bonding type (O(12)), one direct μ-bridging type (O(11)), one terminal atom (O(1)), and one oxygen atom that does not bond to atoms other than the carboxylic carbon atom (O(2)). The delocalized carboxylate groups of BDCI appear to exhibit similar trends, with atomic charges and total basin volumes of the oxygen atoms being almost identical. The partially localized carboxylate groups are characterized by differences in charge and atomic volume between the constituent oxygen atoms. From a structural point of view, a lengthening

of a C−O bond in a carboxylate group is often interpreted as electron localization at this particular oxygen atom. Surprisingly, we observe that the terminal oxygen atom, O(1), and the direct μ-bridging oxygen atom, O(11), possess slightly smaller dipole moments, atomic basins, and charges than O(2) and O(12), despite forming the longer bonds of asymmetric carboxylate groups.

Although the electron density contains no spin information, it is still of interest to probe empirically if it contains some kind of signature related to the magnetic interactions. Unpaired electrons located in specific orbitals may give rise to valence shell charge concentrations (VSCCs). In Figure 8, isosurface plots of the VSCCs of the cobalt atoms are shown.

When examining the chemical bond directions from cobalt to the oxygen atoms, a charge depletion is observed at all bonds except for O(1) and O(11), where the bonds to Co(1) reach into the region of charge concentration. This may reflect the partly covalent nature of these bonds. It is tempting to speculate that the bridging O(11) atom is responsible for the ferromagnetic ordering of the trimetal chains which begins around 85 K. The ferromagnetic ordering may even be in entire layers via BDCII and the O(11) pathway. The chains or layers then subsequently obtain antiferromagnetic order below 42 K through the O(1) atom and the BDCIII linker.

Conclusion

The experimental charge density of **1** has been determined from multipole modeling of 16 K synchrotron X-ray diffraction data. The study is only possible due to the immense intensity available using third-generation synchrotron insertion devices. A topological analysis of the density provides no evidence for
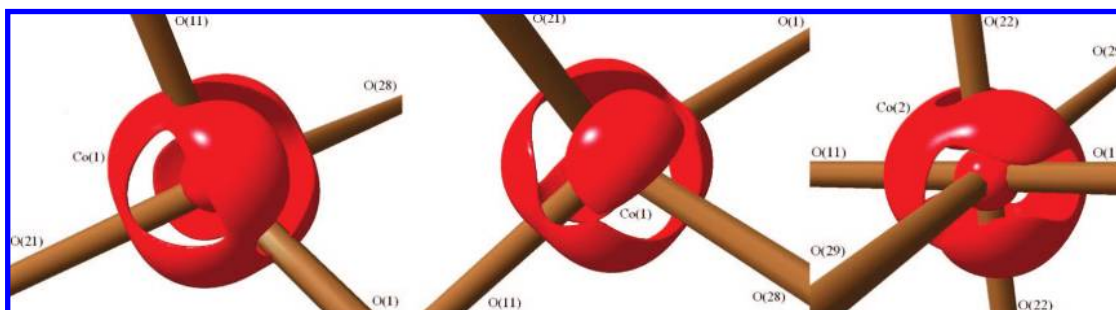
Figure 8. Isosurface plots of the valence shell Laplacian distributions of the two cobalt atoms of **1**: left and middle, the distorted tetrahedral Co(1) atom in two orientations; right, distorted octahedral Co(2). The regions of minimum Laplacian (charge concentration) are shown with $\nabla^2\rho < -900$ e Å^{-5}. The plots were prepared using the program MolIso.[29]

a direct metal−metal interaction, suggesting that the magnetic ordering takes place via superexchange. The metal−ligand bonds are all of closed-shell type, except for the Co(1)−O(1) and the Co(1)−O(11) bonds, which have clear covalent contributions to the bonding. It is speculated that these two bonds are the key mediators of the magnetic ordering. The integrated properties of the two metal atoms reveal atomic charges of ∼1.9e at both Co sites, even though the atomic basins are of dissimilar sizes. A summation of the atomic charges of the framework resulted unexpectedly in a value close to zero, and substantial charge transfer from framework to guest molecules must take place. Formal charge counting on both the metals and the framework is thus inaccurate, and chemical conclusions based on such values, e.g., about guest inclusions properties of porous networks, should be avoided. The charge distributions of the three unique BDC linkers are quite different, and thus their influence on the nanocavity electrostatic potential is a highly tunable property.

Supporting Information Available: Crystallographic information files (CIF) for the measured data; DMSDA values along bond directions; maps of residual density, static deformation density, and Laplacian of the electron density; selected bond distances and angles; a complete listing of bond critical bonds and integrated atomic properties; and experimental orbital populations. This material is available free of charge via the Internet at http://pubs.acs.org.

JA8007215